remote sensing

MDPI

Article

Dynamic Changes and Driving Factors of the Quality of the Ecological Environment in Sanjiangyuan National Park

Liwei Liu [1,2], Cong Wang [1,2], Shaokun Li [1,2], Xiaohan Zhang [1,2,*] and Mingzhu He [1,2]

[1] Joint International Research Laboratory of Catastrophe Simulation and Systemic Risk Governance, Beijing Normal University, Zhuhai 519087, China; liuliwei@mail.bnu.edu.cn (L.L.)
[2] School of National Safety and Emergency Management, Beijing Normal University, Zhuhai 519087, China
* Correspondence: zhangxiaohan@bnu.edu.cn

Highlights

- Overall ecological improvement masks significant degradation in 42% of the park.
- Ecological quality peaks at moderate precipitation levels, not at maximum rainfall.
- Healthier ecosystems in the park are paradoxically linked to high evapotranspiration.
- A novel detector model pinpoints driver thresholds for precision eco-management.

Abstract

National parks face ecological threats from climate change and human activities. Sanjiangyuan National Park (SNP), a major ecological area in China, lacks a systematic evaluation of its ecological environmental quality changes and their driving factors. This study explores these dynamics to provide a scientific basis for regional ecological management. By constructing the remote sensing ecological index (RSEI) and using the optimal multivariate-stratification geographical detector (OMGD) model, we assessed ecological changes from 2014 to 2024. The results showed the RSEI remained stable at approximately 0.66, peaking at 0.732 in 2022, indicating a general improvement in ecological quality. The vegetation coverage rate (NDVI) increased from 0.591 to 0.680. Driving factor analysis revealed considerable regional variation, with temperature and human activities as the primary drivers. Higher RSEI values were associated with conditions where precipitation was moderate (~100 mm), evapotranspiration levels were high (>50 mm), temperatures were above average (>4 °C), and nighttime light indices were low (<0.6). These findings suggest that specific combinations of these factor thresholds may enhance ecological quality, informing protection strategies for SNP and providing a reference for similar plateau ecosystems.

Keywords: remote sensing ecological index (RSEI); driving factor analysis; optimal multivariate-stratification geographical detector (OMGD); Sanjiangyuan National Park (SNP)

check for updates

Academic Editor: Arturo Sanchez-Azofeifa

Received: 16 September 2025
Revised: 24 October 2025
Accepted: 27 October 2025
Published: 30 October 2025

Citation: Liu, L.; Wang, C.; Li, S.; Zhang, X.; He, M. Dynamic Changes and Driving Factors of the Quality of the Ecological Environment in Sanjiangyuan National Park. *Remote Sens.* **2025**, *17*, 3587. https://doi.org/10.3390/rs17213587

Copyright: © 2025 by the authors. Licensee MDPI, Basel, Switzerland. This article is an open access article distributed under the terms and conditions of the Creative Commons Attribution (CC BY) license (https://creativecommons.org/licenses/by/4.0/).

1. Introduction

The International Union for Conservation of Nature (IUCN) defines a national park as "a large natural or near-natural area" with the dual objective of protecting natural ecosystems and providing opportunities for public recreation. These goals highlight the ecological safety and conservation functions of national parks [1]. In recent years, climate change [2,3] and the ongoing degradation of grasslands [4,5] have significantly impacted the ecological environmental quality of the Sanjiangyuan region. Issues such as soil

erosion [6,7], loss of biodiversity [8,9], and deterioration in the habitat quality of flora and fauna [10] have been worsening, directly threatening the stability of the regional ecosystem and indirectly affecting the ecological environmental quality of surrounding rivers and bodies of water. The vulnerability of the ecological environment of the Sanjiangyuan region, which is a crucial "ecological source", is becoming increasingly evident. In response, China proposed a "general plan for establishing a national park system" in 2017, following an exploration of the idea across various nature reserves, and officially established the first batch of national parks in 2021, including Sanjiangyuan National Park (SNP) [11]. Located in the core area of Sanjiangyuan, this park serves as a crucial ecological conservation area for both China and Southeast Asia, playing a crucial role in maintaining regional ecological security. The park encompasses a vast area with complex terrain. In recent years, in the context of climate change, the response of the overall ecological quality in SNP remains unknown, and the pathways of the driving forces are unclear. Therefore, it is imperative to conduct dynamic monitoring of the quality of the ecological environment and analyze the driving forces in this region.

Dynamic monitoring of the quality of the ecological environment is a key way to detect the healthy status of ecosystems, playing a significant role in maintaining regional ecological balance and promoting sustainable development. In recent years, the application of remote sensing technology in environmental research in the Sanjiangyuan region has focused primarily on monitoring grassland degradation based on remote sensing imagery products [12–14], analyzing vegetation dynamic changes [15–17], and estimating carbon stocks [18–20]. However, relatively few evaluations focus on the quality of the ecological environment and analyses of the driving forces of changes in the Sanjiangyuan region have been conducted. The goal of environmental quality assessment is to evaluate the dynamic changes in the structure and function of ecosystems and their quality [21], serving as a critical technical method for quantitatively assessing regional ecological environmental status and its impacts. This research can provide important scientific evidence for regional sustainable economic development and environmental protection policies [22]. In this context, the construction of the remote sensing ecological index (RSEI) provides a tool for the dynamic monitoring and evaluation of the quality of the ecological environment. Xu [23] developed the RSEI by coupling the four indicators including greenness, moisture, dryness, and heat through principal component transformation, successfully addressing the limitations of the traditional ecological index (EI) regarding data acquisition and spatial visualization and significantly improving monitoring efficiency and assessment accuracy. Since then, the RSEI has been widely applied in the field of regional ecological environment monitoring and evaluation [24–26].

Previously, some studies have applied the RSEI to analyze the dynamic changes in the ecological environment quality of SNP. However, these studies have shortcomings in analyzing human-related driving factors and temporal resolution. Moreover, most studies have overlooked the exploration of evapotranspiration, an important biophysical process [27,28]. Given this research background, this study selected four key representative factors to analyze the driving forces. For natural drivers, temperature and precipitation were chosen as they are widely recognized as common and dominant driving factors of ecological environment changes in plateau ecosystems [29,30]. Furthermore, evapotranspiration was added to provide a more complete picture of the water-heat balance. For anthropogenic drivers, the nighttime light index was selected as a quantifiable and spatially explicit proxy for the intensity of human activities and urbanization. While numerous factors can influence the RSEI, these four factors are scientifically justified as representing the primary climatic controls and a key indicator of human disturbance, allowing for a focused analysis that addresses known research gaps.

Additionally, to further analyze the driving mechanism, the optimal multivariate-stratification geographical detector (OMGD) model was introduced to replace the traditional geographical detector (GD) model for driving factor analysis [31]. This model optimizes the discretization of factors, allowing OMGD to utilize interactive detectors to examine the effects of three or more factors, thereby overcoming the two-dimensional limitation in factor interaction analysis.

In this study, the RSEI was employed to conduct a comprehensive assessment of the ecological changes in SNP. The OMGD model was incorporated into the analysis of the driving forces affecting the quality of the ecological environment, the critical threshold parameters for the driving factors across different areas of SNP were identified, and various ecological protection strategies were proposed. This research model not only provides decision support and policy recommendations for ecological construction in SNP but also has implications for the world and other countries, offering valuable guidance for similar plateau ecosystems and national park models. The research framework of this study is shown in Figure 1.

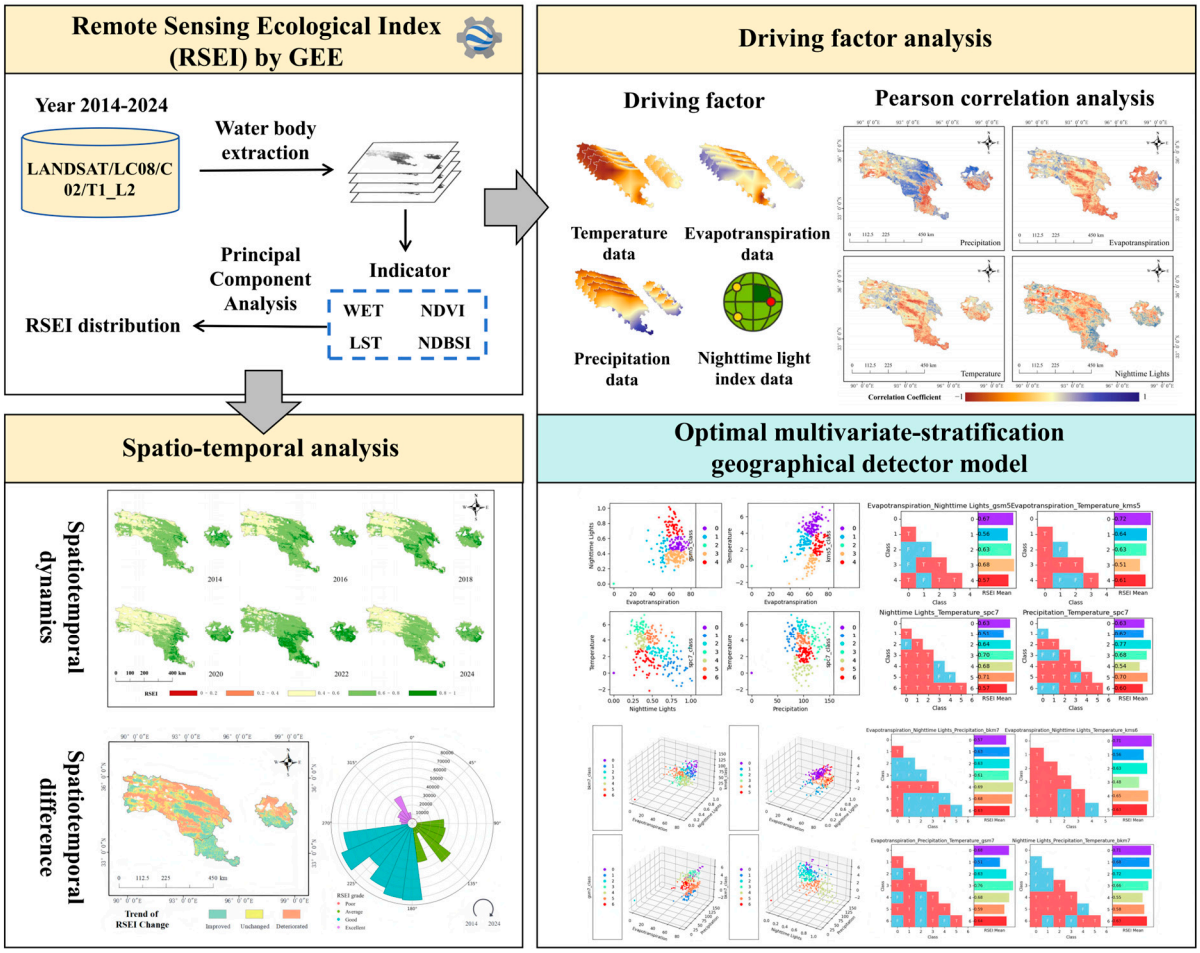


Figure 1. The research framework.

2. Materials and Data

2.1. Study Area

SNP includes the Yangtze River Source Park (YRSP), Huanghe River Source Park (HRSP), and Lancang River Source Park (LRSP), which are located in the northwestern, southern, and eastern parts of the study area, respectively. The geographical coordinates range from 89°50′57″E to 99°14′57″E and 32°22′36″N to 36°47′53″N. The total area of the park is 123,100 km^2, accounting for 31.16% of the total area of the Sanjiangyuan region

(Figure 2). This area encompasses the four counties of Zhiduo, Qumalai, Mado, and Zado, as well as the Kekexili Nature Reserve, which includes 12 towns and 53 administrative villages.

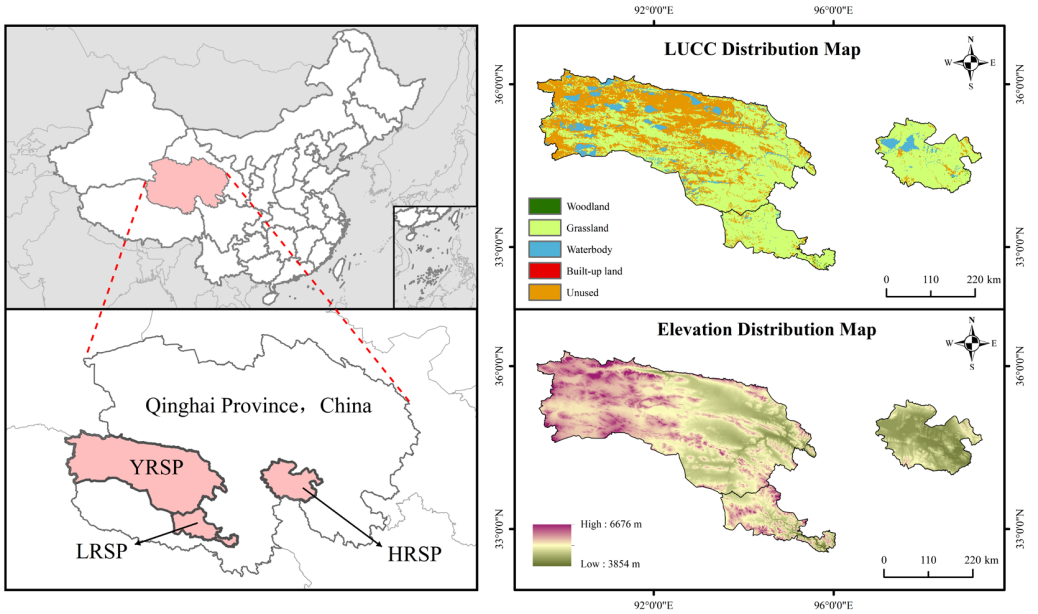


Figure 2. General map of Sanjiangyuan National Park.

Located at the center part of the Tibetan Plateau, this region is characterized primarily by plateaus and high-altitude canyons, the average elevations of which exceed 4500 m. The climate features distinct warm and cold seasons, with rainfall occurring mainly during the warm season. The average annual temperature ranges from −5.6 to 7.8 °C, and the annual precipitation varies from 262.2 to 772.8 mm. The main vegetation types include alpine grasslands and alpine stone slopes, which serve as fundamental ecological resources and play crucial roles in conserving water and maintaining biodiversity in SNP.

2.2. Data Acquisition and Processing

In this study, remote sensing data were obtained from the Google Earth Engine (GEE) JavaScript Code Editor cloud platform, and the RSEI was constructed using Landsat 8 series satellite images. The surface temperature data were sourced from the 'LANDSAT/LC08/C02/T1_L2' dataset, and the calculation of the land surface temperature (LST) directly used the MODIS daily surface temperature and emissivity dataset 'MODIS/061/MOD11A1'. Considering the significant distribution of water bodies within SNP, in this study, the JRC global surface water dataset 'JRC/GSW1_4/YearlyHistory' and the dynamic world high-resolution global land cover dataset 'GOOGLE/DYNAMICWORLD/V1' were integrated for water body extraction. A masking process was then applied to eliminate the water body information to avoid interference with surface moisture conditions and principal component analysis results.

Landsat 8 OLI image data from six years, 2014, 2016, 2018, 2020, 2022, and 2024, were selected, all of which were collected during the vegetation growing season (May to September). To ensure image quality, a cloud masking algorithm was utilized for the preprocessing of surface temperature data, and the minimum cloud cover median synthesis method was employed to obtain the final image data for each target year, effectively reducing the impact of cloud cover on the image analysis.

For the analysis of driving factors, a high-resolution climate and weather dataset, a monthly aggregated version from ERA5, provided by the European Centre for Medium-Range Weather Forecasts (ECMWF) through 'ECMWF/ERA5_LAND/MONTHLY_AGGR', was used.

The nighttime light index was obtained from the dataset 'NOAA/VIIRS/001/VNP46A2'. The vector boundary data for SNP were provided by the Spatiotemporal Big Data Platform for Environmental Studies. The data used are shown in Table 1.

Table 1. Data sources.

Dataset	Source	Temporal Resolution	Spatial Resolution
LANDSAT/LC08/C02/T1_L2	Google Earth Engine	Every 16 days	30 m (spectral bands)
MODIS/061/MOD11A1	Google Earth Engine	Daily (day and night separated)	1000 m
JRC/GSW1_4/YearlyHistory	Google Earth Engine	Annually	30 m
GOOGLE/DYNAMICWORLD/V1	Google Earth Engine	Real-time (synchronized with Sentinel-2 imagery)	10 m
ECMWF/ERA5_LAND/MONTHLY_AGGR	Google Earth Engine	Monthly (average for temperature; cumulative for precipitation/evapotranspiration)	9000 m
NOAA/VIIRS/001/VNP46A2	Google Earth Engine	Daily	500 m
Vector boundary dataset of SNP	Spatiotemporal Big Data Platform	N/A	N/A

3. Methods

3.1. Calculation of the RSEI Component Index

3.1.1. Greenness Index

The greenness index uses the normalized difference vegetation index (NDVI) to represent the vegetation coverage and growth status of a region. The calculation formula is as follows:

$$\mathrm{NDVI} = \frac{\rho_{NIR} - \rho_R}{\rho_{NIR} + \rho_R} \quad (1)$$

In Equation (1), ρ_{NIR} is the reflectance in the near-infrared band, and ρ_R is the reflectance in the red band.

3.1.2. Moisture Index

The moisture index uses the moisture component derived from the tasseled cap transformation to reflect the moisture content (WET) in vegetation, water bodies, and soil, effectively representing the moisture content in the study area. Its expression is as follows [32]:

$$\mathrm{Wet_{OLI}} = 0.1511\rho_2 + 0.1973\rho_3 + 0.3283\rho_4 + 0.3407\rho_5 - 0.7117\rho_6 - 0.4559\rho_7 \quad (2)$$

In Equation (2), $\mathrm{Wet_{OLI}}$ represents the moisture component of Landsat 8 OLI data, and ρ_2 to ρ_7 represent the reflectances of Landsat 8 OLI data in the blue, green, red, near-infrared, shortwave infrared 1, and shortwave infrared 2 bands, respectively.

3.1.3. Dryness Index

The dryness index is the NDBSI, which comprehensively reflects the desiccation phenomenon caused by bare soil and built-up land on the ground. This index is composed of the soil index (*SI*), which represents the degree of dryness of the bare soil, and the *IBI* index, which represents the built-up land. The specific expression of the dryness index (NDBSI) is as follows [33,34]:

$$\mathrm{NDBSI} = (IBI + SI)/2 \quad (3)$$

where

$$IBI = \frac{2\rho_6/(\rho_6 + \rho_5) - [\rho_5/(\rho_5 + \rho_4) + \rho_3/(\rho_3 + \rho_6)]}{2\rho_6/(\rho_6 + \rho_5) + [\rho_5/(\rho_5 + \rho_4) + \rho_3/(\rho_3 + \rho_6)]} \quad (4)$$

$$SI = \frac{(\rho_6 + \rho_4) - (\rho_5 + \rho_2)}{(\rho_6 + \rho_4) + (\rho_5 + \rho_2)} \quad (5)$$

In Equation (3), the NDBSI represents the built-up bare soil index. In Equations (4) and (5), the *IBI* and *SI* represent the built-up index and soil index, respectively. The reflectance values ρ_2 to ρ_7 correspond to the blue, green, red, near-infrared, and shortwave infrared 1 bands of the Landsat 8 data.

3.1.4. Heat Index

The surface temperature representing the heat index is indicated by the temperature corrected for emissivity. The brightness temperature T_b is calculated using the thermal infrared band from Landsat 8 data, followed by correction for emissivity ε. Its expression is as follows [35]:

$$\mathrm{LST} = T_b / [1 + ((\lambda T_b)/\rho) \ln \varepsilon] \quad (6)$$

where [36,37]:

$$T_b = \mathrm{K}_2 / \ln\left(\frac{K_1}{L_6} + 1\right) \quad (7)$$

$$L_6 = in \times DN + bias \quad (8)$$

In Equation (6), the LST represents the built-up heat index; λ denotes the center wavelength of Band 10 of Landsat 8, which is 10.9 μm. ρ equals 1.438×10^{-2} mK; ε represents the emissivity. In Equation (7), K_1 and K_2 are calibration parameters, and T_b is the brightness temperature. In Equation (8), *DN* represents the grayscale value of the Landsat 8 pixel, whereas gain and bias refer to the band gain value and bias value, respectively, with L_6 representing the radiance value of the TIRS thermal infrared band.

3.2. Construction of the RSEI

In this study, PCA was utilized to combine four indicators to form the RSEI, with the first principal component (PC1) chosen to represent the RSEI. The core advantage of this method lies in the fact that the weights of the indicators are not set subjectively but are automatically determined based on their contribution to the principal components, effectively avoiding biases introduced by subjective weighting. The importance of each indicator to the RSEI was weighted according to its loadings on PC1, thus avoiding the subjective weight selection issues commonly encountered in weighting methods. Therefore, the initial RSEI (RSEI_0, i.e., PC1) is represented by:

$$\mathrm{RSEI}_0 = \mathrm{PC1}[f(\mathrm{Wet}, \mathrm{NDVI}, \mathrm{LST}, \mathrm{NDBSI})] \quad (9)$$

If the initial RSEI had a lower value corresponding to good ecological conditions and a higher value corresponding to poor ecological conditions (for example, when the NDVI was negative), then $1 - \mathrm{RSEI}_0$ was used to ensure that the higher values represented better ecological status, as typically expected [38]:

$$\mathrm{RSEI} = 1 - \mathrm{RSEI}_0 = 1 - \mathrm{PC1}[f(\mathrm{Wet}, \mathrm{NDVI}, \mathrm{LST}, \mathrm{NDBSI})] \quad (10)$$

This transformation flipped the scale so that it aligned with the expected interpretation of the ecological conditions, where increased index values indicated improved ecological health.

Notably, the four indicators—NDVI, NDBSI, LST, and Wet—have different dimensions, and performing PCA directly would result in unequal weight allocation among the indicators. Therefore, before implementing PCA, it was necessary to standardize the indicators, converting their values to a uniform range of 0–1. This process not only eliminated the

influence of dimensional differences but also effectively reduced interference caused by temporal factors. The standardization calculation formula is as follows:

$$NI_i = (I_i - I_{min})/(I_{max} - I_{min}) \tag{11}$$

In Equation (11), NI_i represents the standardized results of each indicator, I_i denotes the value of each indicator at pixel i, I_{max} refers to the maximum value of the indicators, and I_{min} refers to the minimum value of the indicators.

After standardizing the four indicators, band synthesis was performed to construct a multidimensional dataset, followed by PCA to extract PC1 and its statistical characteristics. Ultimately, by normalizing PC1, we obtained the standardized RSEI.

3.3. Driving Factor Analysis Method

3.3.1. Pearson Correlation Coefficient

The Pearson correlation coefficient is a statistical tool used to measure the strength and direction of the linear relationship between two variables. In the analysis of the relationship between the RSEI and the driving factors, this coefficient can help evaluate whether a linear relationship exists and the degree of correlation between them. The calculation formula for the Pearson correlation coefficient is as follows:

$$r = \frac{n(\sum xy) - (\sum x)(\sum y)}{\sqrt{\left[n\sum x^2 - (\sum x)^2\right]}} \tag{12}$$

In Equation (12), r represents the Pearson correlation coefficient, n denotes the number of observations, x is the value of the RSEI, and y refers to the value of an individual driving factor.

3.3.2. Optimal Multivariate-Stratification Geographical Detector

In this study, the optimal multivariate-stratification geographical detector (OMGD) model was employed to analyze the relationships between the RSEI and the selected driving factors, revealing spatial heterogeneity and quantifying explanatory power. Compared with the traditional geographic detector (GD), the OMGD model incorporates two additional modules: optimization of factor discretization and scale detection. Our research specifically focused on the factor discretization module. We selected this module because it programmatically optimizes factor discretization by testing a comprehensive suite of built-in methods, as detailed by the model's developers. The approach integrates various variable stratification methods, allowing for the automatic discretization of both single factors and combinations of multiple factors. The built-in suite includes five common univariate methods (natural breaks, quantiles, equal intervals, geometric intervals, and standard deviations) and five robust clustering-based stratification methods (K-means, bisecting K-means, agglomerative clustering, spectral clustering, and Gaussian mixture models). Such a specific combination is a key feature designed to effectively handle both single factors and the multi-factor combinations analyzed in our study.

The optimized factor discretization approach enables OMGD to utilize interaction detectors to assess the influence of three or more factors, overcoming the two-dimensional limitations associated with factor interaction analysis. Additionally, the OMGD model provides user-friendly visualization features, facilitating more in-depth exploratory analysis and result interpretation.

OMGD uses the q statistic to quantify spatial differences, identify explanatory factors, and analyze interactions between variables. The expression for q is as follows:

$$q = 1 - \frac{\sum_{h-1}^{L} N_h \sigma_h^2}{N\sigma^2} \quad (13)$$

In Equation (13), L represents the number of strata for the explanatory variables, N_h denotes the number of observations in the h-th stratum of the explanatory variable, ${\sigma_h}^2$ indicates the variance of the dependent variable in the h-th stratum, and N and σ^2 represent the total number of observations and the variance of the dependent variable across all observations, respectively. Based on the q statistic, this model can automatically explore the optimal discretization schemes for single factors or combinations of multiple factors.

4. Results

4.1. Principal Component Analysis Results of the Ecological Environment Indicators

Table 2 presents the results of the first principal component (PC1) analysis for the four indicators over the six selected years. The rows "Wet", "NDVI", "LST" and "NDBSI" in the header correspond to the moisture index, greenness index, heat index and dryness index introduced in Section 3.1 respectively. The loadings on PC1 are ecologically significant and justify its use for the RSEI. In most years (2016–2024), the NDVI shows a positive loading, while the LST consistently shows a strong negative loading. This aligns with the expected reality that vegetation enhances ecological quality, while excessive surface heat degrades it. The WET indicator generally shows a small negative loading, and the NDBSI loading is minimal.

Table 2. The results of PC1 in principal component analysis.

Parameters	2014	2016	2018	2020	2022	2024
Wet	0.115	−0.156	−0.113	0.059	−0.090	−0.116
NDVI	−0.539	0.283	0.384	0.942	0.600	0.722
LST	0.834	−0.946	−0.916	−0.319	−0.795	−0.680
NDBSI	−0.025	0.000	0.003	0.084	0.000	0.051
Eigenvalue	0.008	0.009	0.008	0.008	0.007	0.008
Percent eigenvalue/%	59.15	67.04	65.27	51.94	58.21	59.42

A notable exception is 2014, where the NDVI loading was negative (−0.539) and the LST loading was positive (0.834). As described in our methodology (Section 3.2), this inversion required the initial $RSEI_0$ to be subtracted from 1. This transformation ensures that the final RSEI value consistently represents ecological quality, where higher values indicate better conditions.

Compared to other components, PC1 effectively encapsulates the characteristic information of all four indicators into a single metric. Although the proportion of information (eigenvalue percentage) ranges from 51.94% to 67.04%, it represents the most significant combined ecological information [39]. The specific numerical loadings for PC2-PC4, which show more complex and varied contributions from the indicators, are provided in Appendix A, Tables A1–A3.

4.2. Spatiotemporal Dynamics of Ecological Quality

Over the past decade, the ecological quality of SNP has shown a stable and gradually improving trend. The RSEI remained consistently high, with a mean value of approximately 0.66, and peaked at 0.732 in 2022. This overall improvement was primarily driven by a significant increase in vegetation coverage, as the mean NDVI rose from 0.591 in 2014 to

0.680 in 2024. In contrast, other indicators such as the WET and LST remained relatively stable, while the NDBSI exhibited considerable fluctuation over the period. The low volatility in most indicators, evidenced by stable standard deviations, suggests a balanced and steady ecological restoration process (detailed statistics for all indicators are provided in Appendix A, Table A4).

The spatial distribution of ecological quality, visualized in Figure 3, confirms these positive changes. Throughout the study period, there was a consistent decrease in areas classified as having 'poor' and 'very poor' ecological quality (represented by red and orange colors). Concurrently, areas of 'good' and 'excellent' quality (light and dark green colors) expanded significantly, especially after 2016. This spatial trend, which peaked in 2022, indicates that environmental restoration measures have had a tangible and positive impact on the regional ecological quality of SNP.

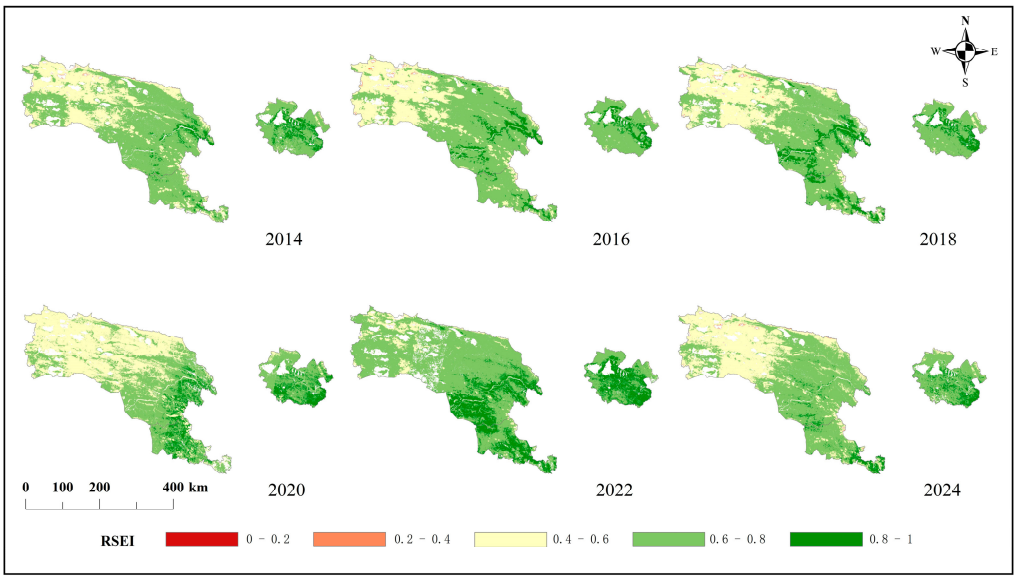


Figure 3. RSEI map of SNP, 2014–2024.

4.3. Spatiotemporal Difference Analysis of Ecological Quality

To analyze the spatiotemporal changes in the ecological quality of SNP over the past decade, a linear regression analysis of RSEI values was conducted on a per-pixel basis based on the RSEI. The resulting trend of the RSEI values is shown in Figure 4. From 2014 to 2024, the area with stable or slightly changing ecological conditions in SNP was 28,566.84 km^2, accounting for 24.53% of the total area; the area with improved ecological conditions was 39,378.95 km^2, accounting for 33.82%; and the area with deteriorating ecological conditions was 48,500.30 km^2, accounting for 41.65% of the total area. Regions experiencing ecological degradation are distributed mainly in the northern parts of the YRSP and HRSP, while the areas of improvement are located primarily in the southern part of the HRSP and in the LRSP, which are regions with extensive grasslands and alpine grasslands.

Ecological degradation in the YRSP and HRSP is primarily driven by permafrost degradation and intensive grazing. Rising temperatures have deepened the active layer and accelerated permafrost thawing, leading to thermokarst formation, wetland shrinkage, and altered soil moisture and hydrological processes, which reduce vegetation cover and ecosystem resilience [40,41]. Meanwhile, concentrated grazing during the growing season removes biomass, compacts soil, decreases organic carbon, and enhances surface runoff and erosion, further aggravating vegetation and soil degradation [42,43]. The interaction between permafrost thaw and overgrazing forms a positive feedback that amplifies ecological deterioration by weakening vegetation's capacity to buffer thermal

and hydrological stress, resulting in sustained declines in vegetation productivity and soil quality in the headwater regions of the Yangtze and Yellow Rivers.

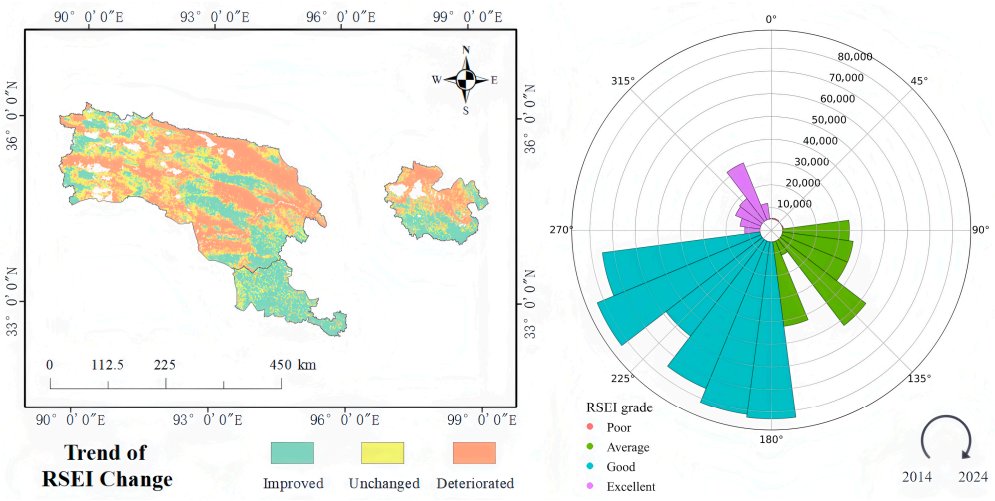


Figure 4. Spatiotemporal variation map of the RSEI in SNP from 2014 to 2024.

The right side of Figure 4 shows a circular bar chart depicting the changes in the area of each RSEI level in SNP over the years. In this chart, the height of the bars represents the area (km^2). From 2014 to 2024, the combined area of poor and very poor ecological levels remained below 0.4% of the total area. The proportions of moderate and good ecological levels were relatively high, stabilizing between 25.73% and 41.84% and between 47.01% and 69.70%, respectively. Moreover, the proportion of excellent levels gradually increased from 5.86% in 2014 to 24.20% in 2022, indicating a steady expansion of high-quality ecological areas.

4.4. Response of Ecological Quality to the Driving Factors

4.4.1. Pearson Correlation Analysis

To explore the relationship between ecological quality and its potential drivers, we performed a Pearson correlation analysis between the RSEI and four key factors selected for this study: precipitation, evapotranspiration, temperature, and the nighttime light index. As justified in the introduction, these factors represent the region's dominant climatic drivers and a primary proxy for human activity. These driving factors exhibited significant spatial heterogeneity across SNP, as detailed in the Appendix A, Figures A1–A3.

The correlation analysis revealed distinct spatial patterns, as shown in Figure 5. Overall, the RSEI was positively correlated with precipitation and temperature, while it showed a negative correlation with evapotranspiration and the nighttime light index. The correlation between temperature and the RSEI was primarily positive in the high-altitude areas, indicating that the limiting effects of low temperatures on ecosystems were mitigated [44]. In cold high-altitude regions, rising temperatures can improve vegetation, water-heat conditions, and biological activity, significantly enhancing the quality and productivity of the ecosystem, and this was reflected in the increase in RSEI values in this study. Similarly, the positive correlation with precipitation was strongest in the YRSP.

Conversely, the negative correlation between the RSEI and evapotranspiration was most pronounced in the grassland regions of the LRSP and HRSP, suggesting that these ecosystems are particularly sensitive to the local water balance. Critically, the nighttime light index showed a strong negative correlation with ecological quality, reflecting the adverse impacts of human activities and urbanization on the ecosystem's health.

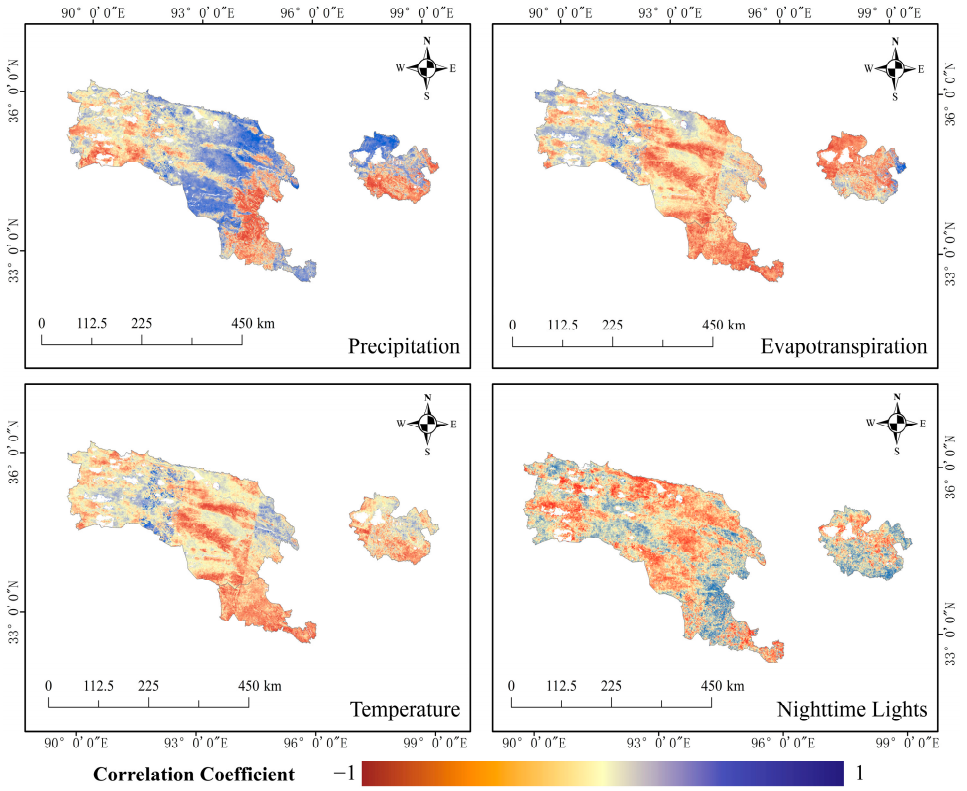


Figure 5. Distribution map of the RSEI and climate driver correlations.

4.4.2. Optimal Multivariate-Stratification Geographical Detector Model

Although the Pearson correlation coefficient effectively quantifies the strength of linear associations between variables, it has limitations in analyzing spatial heterogeneity and representing multifactor interaction effects. In this study, the OMGD model was employed; it not only quantified the explanatory power of single or dual variables on the spatial differentiation of the RSEI but also overcame the limitations of traditional geographical detectors by quantifying the spatial scale effects of three variables on the ecological environment.

The results of the factor detection analysis indicate that temperature is the dominant driver (q = 0.1631, $p < 0.01$), followed by the nighttime light factor (q = 0.0773, $p < 0.01$), suggesting that temperature and human activities are the dominant driving factors. In contrast, the statistical significance of the precipitation and evapotranspiration factors was insufficient, indicating weaker explanatory power.

For the case of dual-factor combinations, the interaction factor detection results are as follows: evapotranspiration ∩ temperature (q = 0.1911, $p < 0.01$) > precipitation ∩ temperature (q = 0.1869, $p < 0.01$) > nighttime light ∩ temperature (q = 0.1716, $p < 0.01$) > evapotranspiration ∩ nighttime light (q = 0.0959, $p < 0.01$). The q values of the interaction results indicate that the explanatory power of the interaction between nighttime light and temperature was greater than that of their individual effects, indicating dual-factor enhancement. Among the other three results, the explanatory power of any two interacting influencing factors was greater than the sum of their individual effects, indicating nonlinear enhancement. This suggests that changes in ecological quality result from the combined effects of multiple factors. Moreover, based on the q values, the top three rankings were all combinations of temperature with other factors, indicating that temperature is an important independent driving factor and significantly amplifies its impact on environmental quality through complex coupling mechanisms with other climate and human activity factors.

The risk detection results for the dual-factor combinations are shown in Figure 6a. By combining the category divisions from the factor discretization scatter plots with the mean RSEI values for each category in the risk detector, the following results were obtained: when precipitation was moderate (approximately 100 mm), evapotranspiration levels were high (greater than 50 mm), temperatures were elevated (above 4 °C), and nighttime light indices were low (below 0.6), then the RSEI values were high. Conversely, when the temperature was low (below 2 °C) and the nighttime light index was high (above 0.8), the RSEI values were low, indicating a greater risk to ecological quality.

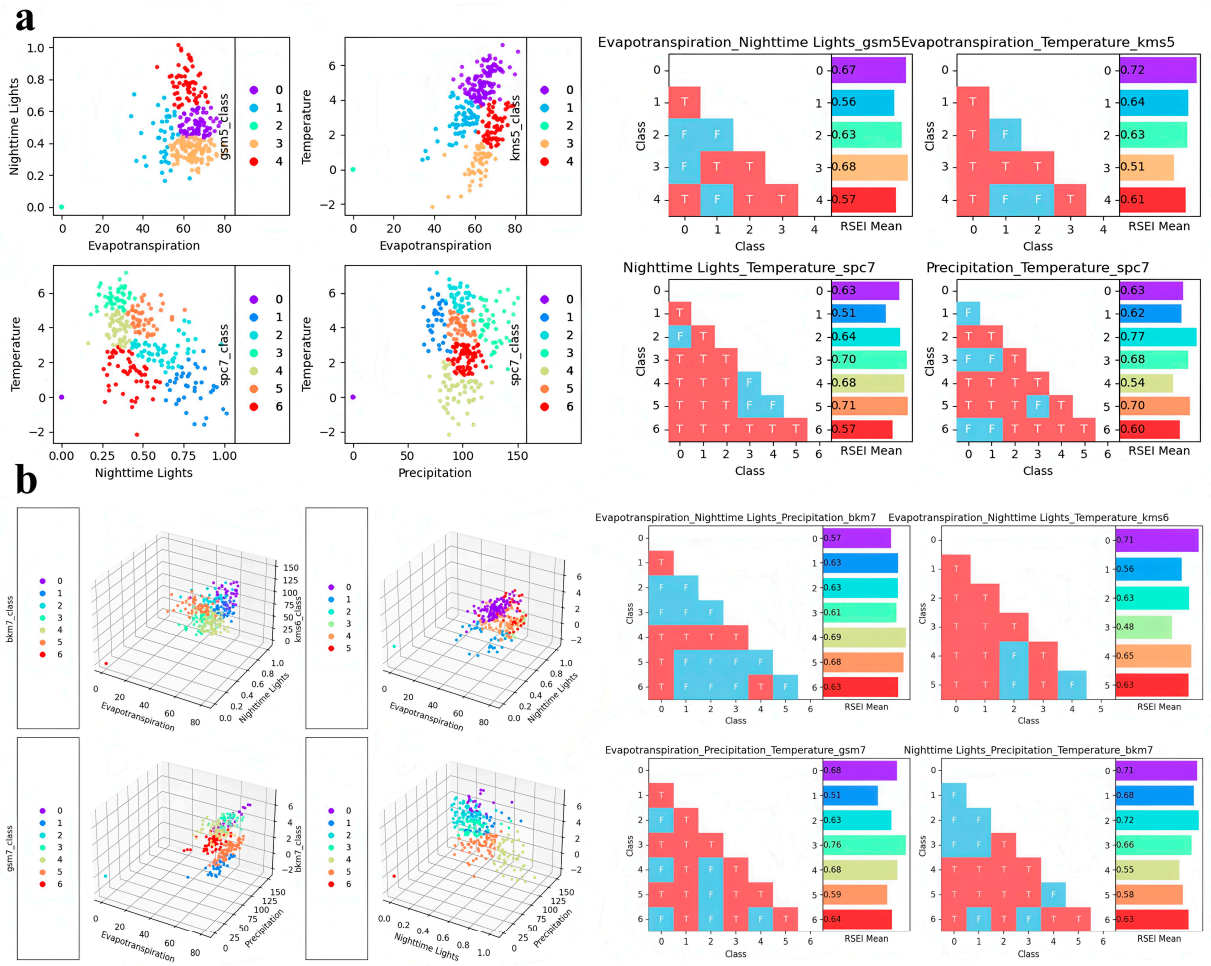


Figure 6. Optimal factor discretization and risk detector results for two- and three-factor combinations ((**a**,**b**), respectively). Note: "Jnb," "qt," "uni," "gmt," and "std" represent the natural breaks, quantile, equal interval, geometric interval, and standard deviation classification methods, respectively, whereas "km," "bkm," "agg," "spc," and "gsm" represent the K-means, bisecting K-means, agglomerative clustering, spectral clustering, and Gaussian mixture model classification methods, respectively. The numbers following the methods indicate the number of categories. For example, gsm5 indicates that the Gaussian mixture model classification method was used to divide the explanatory variables into 5 categories [31]. In the figure, "T" indicates that there is a significant difference between the mean values of the dependent variables in the two compared sub-regions, while "F" indicates that there is no significant difference between the mean values of the dependent variables in the two compared sub-regions.

For the three-factor combinations, the interaction factor detection results are as follows: evapotranspiration ∩ precipitation ∩ temperature (q = 0.1839, $p < 0.01$) > evapotranspiration ∩ nighttime light ∩ temperature (q = 0.1628, $p < 0.01$) > nighttime light ∩ precipitation ∩ temperature (q = 0.1410, $p < 0.01$) > evapotranspiration ∩ nighttime light ∩ precipitation (q = 0.0636, $p < 0.05$). Compared with the interaction factor detection results of the

dual-factor combinations, precipitation exhibited a nonlinear reduction effect as a single factor in all three-factor combination results. This suggests that the impact of precipitation on the ecological quality of SNP is not a linear increase or decrease but rather gradually diminishes its incremental effect after reaching a certain threshold. Combined with the analysis of the dual-factor combination results, this threshold is approximately 100 mm. The risk detection results for the three-factor combinations are shown in Figure 6b, and the threshold levels obtained from the analysis of each factor are completely consistent with the results of the dual-factor combinations.

5. Discussion

5.1. Spatiotemporal Dynamics of the Ecological Environment Quality of SNP

The results of this study indicate that the ecological environmental quality of SNP has generally stabilized and improved. The RSEI has remained stable at approximately 0.66 over the past decade, peaking at 0.732 in 2022, suggesting a gradual improvement in regional ecological quality. This improvement may be closely related to the ecological civilization construction action proposed by China in 2012 [45]. Specifically, the mean NDVI increased significantly from 0.591 to 0.680 over the ten years, serving as a core contributing factor to ecological restoration. This upward trend aligns with existing research findings [46]. This change may be associated with the Ecological Protection and Restoration Project (EPRP), which is the largest conservation and restoration project in China's nature reserves, initiated in the Sanjiangyuan area in 2005. Studies have shown that, after the implementation of the EPRP, vegetation coverage, evaluated using NDVI as an indicator, increased by 11.2% [47].

5.2. Analysis of Driving Factors

The results indicate that, overall, the RSEI is positively correlated with precipitation and temperature and negatively correlated with evapotranspiration and the nighttime light index, with temperature and nighttime light being the dominant driving factors. Other studies have shown that the ecological environment quality of SNP is significantly influenced by precipitation and temperature [28], which aligns with the conclusions of this study. However, these studies indicate a slightly negative but not significant relationship between ecological quality and human activities, which differs from the significant negative impact found in this research. This discrepancy in the analytical results may be attributed to the different driving factors selected for evaluating human impacts.

The association between high evapotranspiration levels (greater than 50 mm) and the improvement in the RSEI may be attributed to the temporal lag of the RSEI. For example, a region with a high RSEI value may have experienced greater precipitation a month earlier, resulting in favorable vegetation growth conditions, indicating that the RSEI is related to the driving factors from a prior period. However, the driving factor data selected in this study coincided with the data used to calculate the RSEI, which could lead to a lag in the correlation response. From this perspective, the association between relatively high evapotranspiration levels and the improvement in the RSEI may suggest that certain regions have relatively high levels of ecosystem health (as reflected by the RSEI) and possibly sufficient soil moisture content, supporting increased evapotranspiration activities [48]. Additionally, the phenomenon of precipitation exhibiting a nonlinear diminishing effect with a threshold of 100 mm may be closely related to the ecosystem's ability to adapt to excess moisture [49], plant growth conditions, and soil erosion factors. To further explain this phenomenon, it is essential to consider multiple factors comprehensively and conduct detailed field investigations and data analyses.

5.3. Recommendations for the Ecological Environmental Protection of SNP

In this study, the optimal multivariate-stratification geographical detector (OMGD) model was introduced into the analysis of driving factors for changes in ecological environmental quality, and it was used to obtain the thresholds for the significant impacts of various driving factors on the RSEI. By integrating the results of the Pearson correlation analysis with the different climates and human activities of the three parks, specific ecological environmental protection strategies can be proposed for each park. Based on the following strategies, SNP can be further delineated into vulnerable risk areas to identify focal points for further ecological environmental protection:

1. For the YRSP, the temperature in the northwestern region is low, but the main land use type in this area is grassland, which may lead to ongoing degradation of the grasslands. Therefore, this area should receive focused attention, and ecological measures such as restricting grazing, rotational grazing, intensive livestock farming, and artificial seeding should be implemented to reduce and restore degraded grasslands, along with ongoing monitoring. With the temperature impacts caused by climate change, the monitoring area also needs to undergo dynamic updates. In addition, the overall correlation results of the nighttime light index in the YRSP indicate that human activities exert excessive pressure on the ecological environment. To address this, the residential and arable land areas within the park should be controlled, illegal farming should be prohibited, and the outward migration of residents should be encouraged, gradually relocating people from the core protected area.
2. For the HRSP, the temperature in the northwestern region is low, and the same protection strategies as those implemented in the northwestern region of the YRSP should be adopted. Furthermore, the total annual precipitation in this area is insufficient (less than 80 mm), necessitating the establishment of a monitoring system to assess water resources and soil quality regularly for timely adjustments to protection measures. Wetlands play a crucial role in regulating the water cycle, and efforts should be made to enhance the protection and restoration of wetlands in this area. Regarding human activities, land use planning should be developed to limit agricultural development in this area, and consideration should be given to implementing grassland restoration projects to protect natural ecosystems and vegetation.
3. For the LRSP, the temperature in the central region is low, necessitating the implementation of the same protection strategies as those used in the northwest region of the YRSP. Additionally, this area receives relatively high total annual precipitation (greater than 120 mm), so a combination of measures such as vegetation restoration, soil and water conservation, restricted grazing, and rotational grazing should be employed to reduce soil erosion. A monitoring system should also be established to evaluate and adjust these measures regularly, promoting the sustainable development of the ecosystem.

To ensure the effectiveness of these strategies and enhance their practical guiding value, we strongly recommend establishing a dynamic monitoring and effect evaluation framework, in order to quantitatively assess the impact of the proposed protection measures. This framework would involve continuous baseline establishment by monitoring the RSEI within the target protection zones to track ecological quality changes against the established pre-policy baseline. This would be combined with a comparative impact assessment, which requires designating specific policy implementation zones alongside control zones (areas with similar ecological, climatic, and socio-economic baselines but which do not receive the new interventions). By tracking the RSEI trajectories in both types of zones, it becomes possible to quantitatively distinguish policy-induced ecological changes from broader climatic or natural trends. This evaluation provides a robust, evidence-based

method to determine which strategies are effective and should be scaled up, and which require modification.

5.4. Limitations and Future Research Directions

In this study, only the driving factor data that corresponded to the period of the data used were selected to calculate the RSEI. As discussed in Section 5.2, this approach may overlook the temporal lag of the RSEI, leading to biased results in the driving factor analysis. Therefore, future research should consider the time intervals at which the various driving factors affect the RSEI and select appropriate driving factor data within suitable time ranges.

Due to limitations in data sources, in this study, only the nighttime light index was used to represent the level of human activity interference in SNP. Although the nighttime light index can reflect certain impacts of human activities to some extent, it is not comprehensive. Human activities that are not reflected in the nighttime light index include traffic flow, tourism, residential migration, and various ecological protection and restoration projects. Future research should incorporate a broader range of human activity variables to provide a more comprehensive understanding of the driving factors behind ecological changes. Additionally, in this study, analyses were conducted over a nearly 10-year timeframe; the use of a shorter timeframe may reduce the significance of the results. Future research could incorporate previous or updated data analysis results in combination with the findings of this study to gain deeper insights into the changing trends in the ecological quality of SNP.

Furthermore, this study faced a challenge regarding the spatial resolution mismatch between the RSEI data (30 m) and the driving factor data. As shown in Table 1, the climate data and nighttime light data have much coarser spatial resolutions (9000 m and 500 m, respectively). In our analysis, we resampled these coarser driving factor datasets to the 30 m resolution of the RSEI. This resampling process, while methodologically necessary, introduces uncertainty. Applying coarse-scale climate or human activity data to fine-scale ecological pixels might obscure local variations and impacts, potentially affecting the precise quantitative results of the driving factor analysis. Future research should endeavor to utilize higher-resolution or statistically downscaled driving factor datasets, where available, to mitigate this spatial scale mismatch.

6. Conclusions

This study assessed the ecological environmental quality of Sanjiangyuan National Park (SNP) from 2014 to 2024 using the RSEI and identified its key drivers with the OMGD model. The main conclusions are as follows:

1. The ecological environmental quality of SNP showed a generally stable and improving trend, with the RSEI peaking in 2022. This improvement was primarily driven by a significant increase in vegetation coverage (NDVI).
2. Driving factor analysis identified temperature and human activities as the dominant factors influencing the spatial differentiation of RSEI. Temperature not only had a strong independent effect but also amplified its impact when interacting with other factors.
3. The study successfully identified optimal environmental thresholds for high ecological quality: moderate precipitation (~100 mm), high evapotranspiration (>50 mm), elevated temperatures (>4 °C), and low human activity (<0.6 nighttime light index).

Based on these findings, targeted ecological protection strategies were proposed for the different regions of the park, coupled with a recommendation for a dynamic evaluation framework to quantitatively assess their effectiveness. This research provides a scientific

basis for policy-making in SNP and offers a methodological reference for other high-altitude protected areas.

Author Contributions: Conceptualization, X.Z., M.H. and L.L.; methodology, L.L.; software, L.L.; validation, X.Z., M.H. and L.L.; formal analysis, L.L., C.W. and S.L.; investigation, L.L.; resources, L.L.; data curation, L.L.; writing—original draft preparation, L.L.; writing—review and editing, L.L., C.W., S.L., X.Z. and M.H.; visualization, L.L.; supervision, X.Z. and M.H.; project administration, X.Z. and M.H.; funding acquisition, X.Z. All authors have read and agreed to the published version of the manuscript.

Funding: This research was supported by the National Natural Science Foundation of China [Grant no: 42471114], Fundamental Research Funds for the Central Universities (124330008) and the Beijing Normal University Research Start-up Funding for Talent (No. 310432104). The financial support is gratefully acknowledged.

Data Availability Statement: The data sources are listed in the text.

Acknowledgments: Thanks support from the Interdisciplinary Intelligence Super Computer Center of Beijing Normal University at Zhuhai. During the preparation of this manuscript, the author(s) used Gemini 2.5 Pro, a large language model developed by Google, for the purposes of distilling key arguments and editing text. The authors have reviewed and edited the output and take full responsibility for the content of this publication.

Conflicts of Interest: The authors declare that they have no known competing financial interests or personal relationships that could have appeared to influence the work reported in this paper.

Appendix A

Table A1. The results of PC2 in principal component analysis.

Parameters	2014	2016	2018	2020	2022	2024
Wet	−0.053	0.075	−0.079	−0.146	−0.131	−0.153
NDVI	−0.837	−0.952	−0.922	−0.305	−0.798	−0.683
LST	−0.537	−0.297	−0.377	−0.940	−0.588	−0.707
NDBSI	−0.094	0.000	−0.044	−0.042	−0.001	−0.098
Eigenvalue	0.004	0.003	0.003	0.006	0.004	0.004
Percent eigenvalue/%	30.080	25.140	25.100	38.750	33.160	31.730

Table A2. The results of PC3 in principal component analysis.

Parameters	2014	2016	2018	2020	2022	2024
Wet	0.944	−0.985	−0.984	0.964	0.987	0.947
NDVI	−0.011	−0.117	0.034	−0.120	−0.051	−0.048
LST	−0.128	0.127	0.135	−0.120	−0.151	−0.194
NDBSI	0.305	0.000	−0.112	0.205	0.002	0.251
Eigenvalue	0.001	0.001	0.001	0.001	0.001	0.001
Percent eigenvalue/%	10.600	7.820	9.600	9.250	8.630	8.730

Table A3. The results of PC4 in principal component analysis.

Parameters	2014	2016	2018	2020	2022	2024
Wet	−0.306	0.000	0.114	0.214	−0.002	−0.257
NDVI	−0.093	0.000	0.039	0.069	−0.001	−0.096
LST	0.010	0.000	−0.002	−0.012	0.000	0.015
NDBSI	0.948	1.000	−0.993	−0.974	1.000	0.962
Eigenvalue	0.000	0.000	0.000	0.000	0.000	0.000
Percent eigenvalue/%	0.170	0.000	0.020	0.060	0.000	0.120

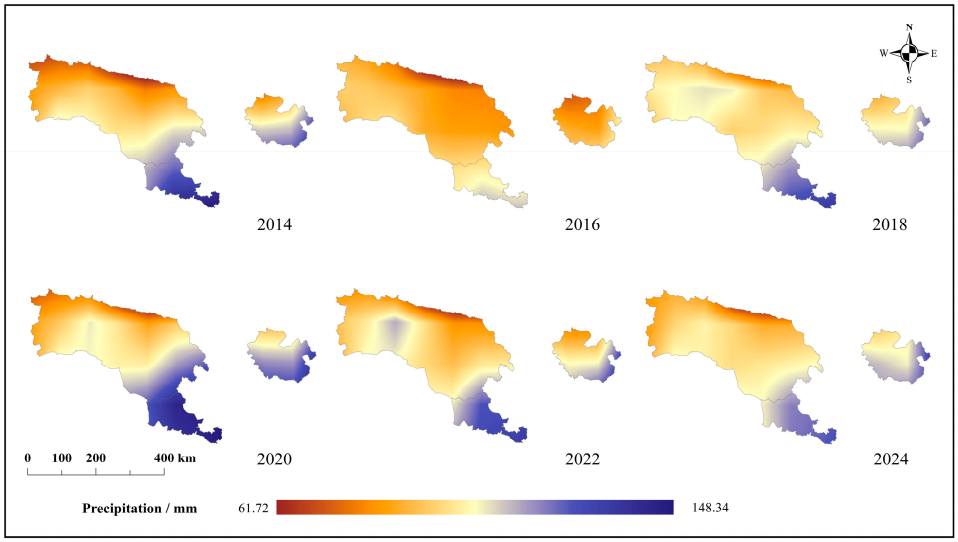


Figure A1. Average precipitation distribution map of SNP, 2014–2024.

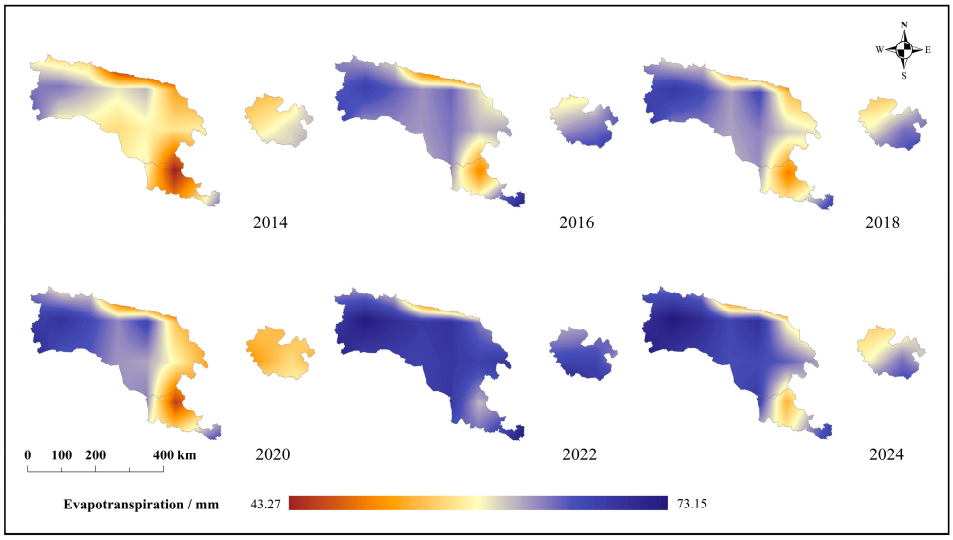


Figure A2. Average evapotranspiration distribution map of SNP, 2014–2024.

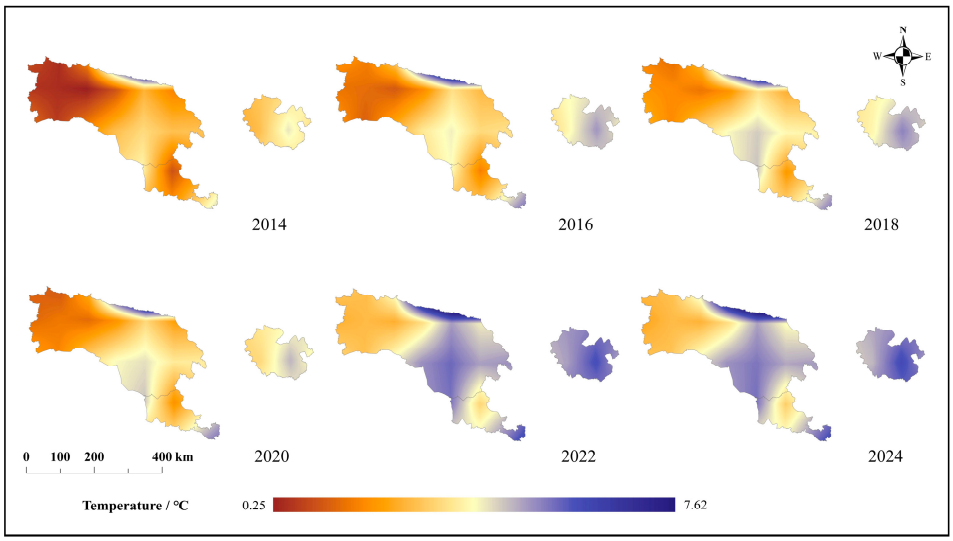


Figure A3. Average temperature distribution map of SNP, 2014–2024.

Table A4. Statistics of the four indicators and the RSEI.

Parameters		Wet	NDVI	LST	NDBSI	RSEI
2014	Mean	0.166	0.591	0.247	0.754	0.663
	Std Dev	0.036	0.074	0.088	0.014	0.090
	Loadings of PC1	0.115	−0.539	0.834	−0.025	—
2016	Mean	0.238	0.606	0.317	0.305	0.666
	Std Dev	0.037	0.067	0.097	0.001	0.101
	Loadings of PC1	−0.156	0.283	−0.946	0.000	—
2018	Mean	0.180	0.644	0.301	0.443	0.671
	Std Dev	0.037	0.068	0.094	0.005	0.106
	Loadings of PC1	−0.113	0.384	−0.916	0.003	—
2020	Mean	0.197	0.644	0.263	0.702	0.647
	Std Dev	0.037	0.093	0.088	0.012	0.100
	Loadings of PC1	0.059	0.942	−0.319	0.084	—
2022	Mean	0.203	0.661	0.243	0.036	0.732
	Std Dev	0.035	0.077	0.083	0.001	0.083
	Loadings of PC1	−0.090	0.600	−0.795	0.000	—
2024	Mean	0.224	0.680	0.248	0.399	0.652
	Std Dev	0.037	0.085	0.085	0.013	0.098
	Loadings of PC1	−0.116	0.722	−0.680	0.051	—

References

1. Shafer, C.L. Cautionary Thoughts on IUCN Protected Area Management Categories V–VI. *Glob. Ecol. Conserv.* **2015**, *3*, 331–348. [CrossRef]
2. Wang, Y.; Lü, Y.; Lü, D.; Yin, L.; Wang, X. Climate Change and Its Ecological Risks Are Spatially Heterogeneous in High-Altitude Region: The Case of Qinghai-Tibet Plateau. *CATENA* **2024**, *243*, 108140. [CrossRef]
3. Cao, W.; Wu, D.; Huang, L.; Liu, L. Spatial and Temporal Variations and Significance Identification of Ecosystem Services in the Sanjiangyuan National Park, China. *Sci. Rep.* **2020**, *10*, 6151. [CrossRef] [PubMed]
4. Chen, X.; Li, Q.; Chen, D.; Zhao, L.; Xiao, C. Stochastic Ecological Processes Assemble Soil Microbial Communities in Degraded Patches of Alpine Grassland in the Sanjiangyuan National Park on the Qinghai-Tibetan Plateau, China. *J. Plant Ecol* **2025**, *18*, rtaf013. [CrossRef]
5. Chen, D.; Li, Q.; Liu, Z.; He, F.; Chen, X.; Xu, S.; Zhao, X.; Zhao, L. Variations of Forage Yield and Nutrients with Altitude Gradients and Their Influencing Factors in Alpine Meadow of Sanjiangyuan, China. *J. Soil. Sci. Plant Nutr.* **2020**, *20*, 2164–2174. [CrossRef]
6. Wang, B.; Gu, Y.; Zhou, K.; Li, S.; Zheng, C.; Lu, Y. Impact of Freeze-Thaw Action on Soil Erodibility in the Permafrost Regions of the Sanjiangyuan Area Affected by Thermokarst Landslides. *Water* **2025**, *17*, 818. [CrossRef]
7. Ma, W.; Hou, S.; Su, W.; Mao, T.; Wang, X.; Liang, T. Estimation of Carbon Stock and Economic Value of Sanjiangyuan National Park, China. *Ecol. Indic.* **2024**, *169*, 112856. [CrossRef]
8. Yang, D.; Liu, Q.; Yang, Z.; Song, J.; Chen, D. Spatiotemporal Dynamics of Human Ecosystems in the Context of Protected Areas as a Policy Tool: Insights from Sanjiangyuan National Park, China. *Ecol. Indic.* **2024**, *165*, 112196. [CrossRef]
9. Li, J.; Yin, H.; Wang, D.; Jiagong, Z.; Lu, Z. Human-Snow Leopard Conflicts in the Sanjiangyuan Region of the Tibetan Plateau. *Biol. Conserv.* **2013**, *166*, 118–123. [CrossRef]
10. Jiang, R.; Liu, J. Characterization and Projection of Spatial and Temporal Changes in Habitat Quality of Sanjiangyuan Based on Land Use Change. *J. Geogr. Sci.* **2024**, *34*, 1797–1821. [CrossRef]
11. Zhao, W. Beginning: China's National Park System. *Natl. Sci. Rev.* **2022**, *9*, nwac150. [CrossRef]
12. Zhang, Q.; Ma, L.; Zhang, Z.; Xu, W.; Zhou, B.; Song, M.; Qiao, A.; Wang, F.; She, Y.; Yang, X.; et al. Ecological restoration of degraded grassland in Qinghai-Tibet alpine region: Degradation status, restoration measures, effects and prospects. *Acta Ecol. Sin.* **2019**, *39*, 7441–7451. [CrossRef]

13. Shang, Z.; Dong, Q.; Shi, J.; Zhou, H.; Dong, S.; Shao, X.; Li, S.; Wang, Y.; Ma, Y.; Ding, L.; et al. Research Progress in Recent Ten Years of Ecological Restoration for 'Black Soil Land' Degraded Grassland on Tibetan Plateau—Concurrently Discuss of Ecological Restoration in Sangjiangyuan Region. *Acta Agrestia Sin.* **2018**, *26*, 1–21.
14. Xu, X.; Wang, L.; Li, J.; Cai, H. Analysis of the Grassland Restoration Trend and Degradation Situation in the "Three-River Headwaters" Region since the Implementation of the Ecological Project. *J. Geo-Inf. Sci.* **2017**, *19*, 50–58.
15. Zhang, X.; He, Y.; Zhao, L. The Spatial-Temporal Variation Characteristics of Vegetation Coverage in Five National Parks from 2000 to 2020. *Nat. Prot. Areas* **2023**, *3*, 11–27.
16. Zhai, X.; Liang, X.; Yan, C.; Xing, X.; Jia, H.; Wei, X.; Feng, K. Vegetation Dynamic Changes and Their Response to Ecological Engineering in the Sanjiangyuan Region of China. *Remote Sens.* **2020**, *12*, 4035. [CrossRef]
17. Zeng, N.; Ren, X.; He, H.; Zhang, L.; Xu, Q.; Zhang, M.; Chen, X.; Gao, C.; Liu, C. Spatial-temporal dynamics of the grassland aboveground biomass and its association with climate changes in the Three River Source National Park. *Acta Ecol. Sin.* **2023**, *43*, 1175–1184. [CrossRef]
18. Jia, T.; Hu, X. Spatial-temporal Change and Driving Force of Carbon Storage in Three-River-Source National Park Based on PLUS-InVEST-Geodector Model. *Environ. Sci.* **2024**, *45*, 5931–5942. [CrossRef]
19. Zhang, F.; Li, H.; Li, W.; Wang, J.; Yi, L.; Luo, F.; Zhang, G.; Wang, C.; Yang, Y.; Li, Y. The spatial pattern and regional classifications of topsoil organic carbon and total nitrogen density based on boosted regression trees in the Sanjiangyuan National Park. *Acta Ecol. Sin.* **2022**, *42*, 5593–5602. [CrossRef]
20. Wu, X.; Shen, C.; Shi, L.; Wan, Y.; Ding, J.; Wen, Q. Spatio-Temporal Evolution Characteristics and Simulation Prediction of Carbon Storage: A Case Study in Sanjiangyuan Area, China. *Ecol. Inform.* **2024**, *80*, 102485. [CrossRef]
21. Xu, Y.; Zhou, H. A Preliminary Study on Advances in Assessment of Eco-environmental Quality in China. *Arid. Land. Geogr.* **2003**, *26*, 166–172. [CrossRef]
22. Chen, W.; Huang, H.; Tian, Y.; Du, Y. Monitoring and Assessment of the Eco-Environment Quality in the Sanjiangyuan Region based on Google Earth Engine. *J. Geo-Inf. Sci.* **2019**, *21*, 1382–1391.
23. Xu, H. A remote sensing index for assessment of regional ecological changes. *China Environ. Sci.* **2013**, *33*, 889–897.
24. Xiong, Y.; Xu, W.; Lu, N.; Huang, S.; Wu, C.; Wang, L.; Dai, F.; Kou, W. Assessment of Spatial–Temporal Changes of Ecological Environment Quality Based on RSEI and GEE: A Case Study in Erhai Lake Basin, Yunnan Province, China. *Ecol. Indic.* **2021**, *125*, 107518. [CrossRef]
25. Liu, X.; Zhou, Q.; Zhou, L.; Meng, H.; Li, M.; Peng, C. RSEI-Based Dynamic Monitoring of Ecological Quality of the Soil and Water Conservation Functional Area in the Chongqing Section of the Three Gorges Reservoir Area. *Res. Soil. Water Conserv.* **2021**, *28*, 278–286. [CrossRef]
26. Wei, Y.; Qian, J.; Fan, W.; Li, P. Dynamic monitoring of ecological environment quality in Lijiang River Basin based on RSEI. *Sci. Soil. Water Conserv.* **2021**, *19*, 122–131. [CrossRef]
27. Xiao, X.; Chen, Y.; Zhang, Y.; Huang, M.; Li, H. Spatio-Temporal Evolution of Ecological Environment Quality Based on High-Quality Time-Series Data Reconstruction: A Case Study in the Sanjiangyuan Nature Reserve of China. *Sustainability* **2024**, *16*, 6231. [CrossRef]
28. Wen, C.; Long, T.; He, G.; Jiao, W.; Jiang, W. Temporally Enhanced RSEI and Nighttime Lights Reveal Long-Term Ecological Changes and Effective Protection in China's Inaugural National Parks. *Ecol. Indic.* **2025**, *170*, 112981. [CrossRef]
29. Yang, X.; Meng, F.; Fu, P.; Zhang, Y.; Liu, Y. Spatiotemporal Change and Driving Factors of the Eco-Environment Quality in the Yangtze River Basin from 2001 to 2019. *Ecol. Indic.* **2021**, *131*, 108214. [CrossRef]
30. Jiang, L.; Liu, Y.; Wu, S.; Yang, C. Analyzing Ecological Environment Change and Associated Driving Factors in China Based on NDVI Time Series Data. *Ecol. Indic.* **2021**, *129*, 107933. [CrossRef]
31. Guo, Y.; Wu, Z.; Zheng, Z.; Li, X. An Optimal Multivariate-Stratification Geographical Detector Model for Revealing the Impact of Multi-Factor Combinations on the Dependent Variable. *GIScience Remote Sens.* **2024**, *61*, 2422941. [CrossRef]
32. Wang, Y. Evaluation of Lake Wetland Ecotourism Resources Based on Remote Sensing Ecological Index. *Arab. J. Geosci.* **2021**, *14*, 559. [CrossRef]
33. Xu, H. A New Index for Delineating Built-up Land Features in Satellite Imagery. *Int. J. Remote Sens.* **2008**, *29*, 4269–4276. [CrossRef]
34. Roy, P.; Rikimaru, A.; Miyatake, S. Tropical Forest Cover Density Mapping. *Trop. Ecol.* **2002**, *43*, 39–47.
35. Nichol, J. Remote Sensing of Urban Heat Islands by Day and Night. *Photogramm. Eng. Remote Sens.* **2005**, *71*, 613–621. [CrossRef]
36. U.S. Geological Survey. *Landsat 8 (L8) Data Users Handbook, Version 5.0*; U.S. Geological Survey: Reston, VA, USA, 2019; LSDS-1574. Available online: https://d9-wret.s3.us-west-2.amazonaws.com/assets/palladium/production/s3fs-public/atoms/files/LSDS-1574_L8_Data_Users_Handbook-v5.0.pdf (accessed on 27 October 2025).
37. Chander, G.; Markham, B.L.; Helder, D.L. Summary of Current Radiometric Calibration Coefficients for Landsat MSS, TM, ETM+, and EO-1 ALI Sensors. *Remote Sens. Environ.* **2009**, *113*, 893–903. [CrossRef]

38. Xu, H.; Wang, Y.; Guan, H.; Shi, T.; Hu, X. Detecting Ecological Changes with a Remote Sensing Based Ecological Index (RSEI) Produced Time Series and Change Vector Analysis. *Remote Sens.* **2019**, *11*, 2345. [CrossRef]
39. Xu, H.; Deng, W. Rationality Analysis of MRSEI and Its Difference with RSEI. *Remote Sens. Technol. Appl.* **2022**, *37*, 1–7.
40. Jin, X.; Jin, H.; Luo, D.; Sheng, Y.; Wu, Q.; Wu, J.; Wang, W.; Huang, S.; Li, X.; Liang, S.; et al. Impacts of Permafrost Degradation on Hydrology and Vegetation in the Source Area of the Yellow River on Northeastern Qinghai-Tibet Plateau, Southwest China. *Front. Earth Sci.* **2022**, *10*, 845824. [CrossRef]
41. Fang, P.; Wang, T.; Yang, D.; Yang, J.; Tang, L. Permafrost Degradation and Concomitant Hydrological Changes Dominated by Anthropogenic Greenhouse Gas Emissions in the Northeastern Tibetan Plateau. *Geophys. Res. Lett.* **2025**, *52*, e2024GL113679. [CrossRef]
42. Zhou, J.; Niu, J.; Wu, N.; Lu, T. Annual High-Resolution Grazing-Intensity Maps on the Qinghai-Tibet Plateau from 1990 to 2020. *Earth Syst. Sci. Data* **2024**, *16*, 5171–5189. [CrossRef]
43. Huang, X.; Liu, X.; Liao, L.; Li, J.; Luo, G.; Li, B.; Ma, Z.; Wang, Z. Grazing Decreases Carbon Storage in the Qinghai-Tibet Plateau Grasslands. *Commun. Earth Environ.* **2025**, *6*, 198. [CrossRef]
44. Wingler, A.; Hennessy, D. Limitation of Grassland Productivity by Low Temperature and Seasonality of Growth. *Front. Plant Sci.* **2016**, *7*, 1130. [CrossRef] [PubMed]
45. Zhang, L.; Wang, H.; Zhang, W.; Wang, C.; Bao, M.; Liang, T.; Liu, K. Study on the Development Patterns of Ecological Civilization Construction in China: An Empirical Analysis of 324 Prefectural Cities. *J. Clean. Prod.* **2022**, *367*, 132975. [CrossRef]
46. Shen, X.; An, R.; Feng, L.; Ye, N.; Zhu, L.; Li, M. Vegetation Changes in the Three-River Headwaters Region of the Tibetan Plateau of China. *Ecol. Indic.* **2018**, *93*, 804–812. [CrossRef]
47. Zhang, L.; Fan, J.; Zhou, D.; Zhang, H. Ecological Protection and Restoration Program Reduced Grazing Pressure in the Three-River Headwaters Region, China. *Rangel. Ecol. Manag.* **2017**, *70*, 540–548. [CrossRef]
48. Ma, N.; Zhang, Y.; Guo, Y.; Gao, H.; Zhang, H.; Wang, Y. Environmental and Biophysical Controls on the Evapotranspiration over the Highest Alpine Steppe. *J. Hydrol.* **2015**, *529*, 980–992. [CrossRef]
49. Zhang, B.; Zhu, J.; Pan, Q.; Liu, Y.; Chen, S.; Chen, D.; Yan, Y.; Dou, S.; Han, X. Grassland Species Respond Differently to Altered Precipitation Amount and Pattern. *Environ. Exp. Bot.* **2017**, *137*, 166–176. [CrossRef]

Disclaimer/Publisher's Note: The statements, opinions and data contained in all publications are solely those of the individual author(s) and contributor(s) and not of MDPI and/or the editor(s). MDPI and/or the editor(s) disclaim responsibility for any injury to people or property resulting from any ideas, methods, instructions or products referred to in the content.